

Performance evaluation of spaceborne oceanographic lidar for optical properties detection in global ocean

Bingyi Liu^(a), Peizhi Zhu^(a), Junwu Tang^(b), Xiaoquan Song^(a), Songhua Wu^(a, c), Yan He^(d)

^(a) College of Marine Technology, Faculty of Information Science and Engineering, Ocean University of China, Qingdao, 266100, China

^(b) Laoshan Laboratory, Qingdao, 266237, China

^(c) Institute for Advanced Ocean Study, Ocean University of China, Qingdao, 266100, China

^(d) Key Laboratory of Space Laser Communication and Detection Technology, Shanghai Institute of Optics and Fine Mechanics, Chinese Academy of Sciences, Shanghai, 201800, China
liubingyi@ouc.edu.cn

Abstract: Detection of vertical distribution of optical properties in global ocean is of high priority to the study of marine environment and carbon cycle. Lidar has the advantage of measuring profiles of optical properties in the water. In this paper, in order to evaluate and analyze the detection performance of lidar for optical properties in global ocean, a simulator was developed to generate lidar return signal and estimate the detection depth of spaceborne oceanographic lidar with given specifications operating in blue-green spectral region. The global detection capability of spaceborne lidar with various power aperture products and typical operating wavelengths is estimated. The results show the distribution of detection depth depends on both water optical properties and operating wavelength. With the same power aperture product, in the cleanest open ocean, the penetration depth of lidar with a wavelength of 443 nm is the deepest. In most open ocean, the lidar with a wavelength of 486 nm has the maximum propagation ability. The lidar with a wavelength of 532 nm is more suitable for detection in coastal water.

1. Introduction

Spaceborne lidar for oceanography can provide global ocean information, making up for the lack of detection capability of passive observing systems at night and high latitudes [1,2]. Meanwhile, its capability of profiling the seawater optical parameters makes it possible to observe the vertical ocean stratification. Currently, oceanographic lidar has been used to measure chlorophyll concentration [3–5], absorption coefficient of colored dissolved organic matter (CDOM) [6], ocean subsurface backscattering [2,7,8], and particulate organic carbon stocks [1].

The emitted laser energy from oceanographic lidars decays rapidly due to the strong absorption and scattering of seawater. There are some other factors, including the optical properties of the seawater and the laser wavelength, which will also have a significant effect on the intensity of the lidar signals. The maximum detectable depth and the capability to retrieve the profiles of the optical properties will be affected. Therefore, the study of the detection mechanism and the establishment of

an accurate simulation model to evaluate the global detection capability of oceanographic lidar is of great importance.

Based on the lidar equation and the bio-optical models, the backscattering signal and the global single photon maximum detectable depth (SPMDD) of the oceanographic lidar are estimated in this research. The reliability of the simulator is verified by comparing the simulated profiles with measured profiles. The global ocean SPMDDs of oceanographic lidar with different specifications are analyzed.

2. Simulator and data

2.1. Lidar equation

The echo signal profiles of oceanographic lidar can be simulated by the lidar equation,

$$N(z) = K\beta(\pi, z) \exp\left[-2 \int_0^z \alpha(z') dz'\right] \quad (1)$$

where $N(z)$ is the photon counts scattered by the water column received by the detector, $\alpha(z)$ is the lidar attenuation coefficient, and $\beta(\pi, z)$ is the volume scattering coefficient at a scattering angle of π radians. The lidar instrument constant K is expressed as

$$K = \frac{E_0}{h\nu} \frac{A}{(nH+z)^2} T_{\text{atm}}^2 T_{\text{sur}}^2 \eta \Delta z \quad (2)$$

where E_0 is the single pulse energy, h is the Planck constant, ν is the laser frequency, $E_0/h\nu$ is the number of photons emitted, A is the receiving area of the telescope, H is the detection height of the lidar, n is the refractive index of seawater, $A/(nH+z)^2$ is the receiving solid angle, T_{atm} is the atmospheric transmittance, T_{sur} is the air-sea interface transmittance, η is the detection efficiency including optical efficiency and quantum efficiency, and Δz is the vertical resolution.

The parameters in the lidar equation can be determined by the specifications of the oceanographic lidar system except for the optical parameters, α and $\beta(\pi)$, which is calculated by the bio-optical model.

The backscattering signals $N_c(z)$ received by the lidar detector are obtained as

$$N_c(z) = N(z) + N_{\text{sun}} \quad (3)$$

where N_{sun} is calculated by [9]:

$$N_{\text{sun}} = I_b A \Delta \lambda \Delta t \eta \frac{\phi^2 \pi}{4} \frac{\lambda}{h\nu} \quad (4)$$

where I_b is the solar spectral radiance reflected by the atmosphere and sea surface [10], $\Delta \lambda$ is the filter bandwidth of the detector, Δt is the sampling time, ϕ is the field of view and λ is the wavelength. The influence of the number of after-pulse, random noise and dark count photons are ignored.

2.2. Bio-optical model of seawater

Considering the influence of multiple scattering, α and $\beta(\pi)$ are modeled as

$$\alpha = K_d + (c - K_d) \exp(-0.85cD) \quad (5)$$

$$\begin{aligned} \beta(\pi) &= \beta_p(\pi) + \beta_w(\pi) \quad (6) \\ &= \tilde{\beta}_p(\pi) b_p + \tilde{\beta}_w(\pi) b_w \end{aligned}$$

Eq.(5) is based on the approximation of the Monte Carlo simulation [11]. K_d is the diffusion attenuation coefficient of seawater, c is the attenuation coefficient of seawater, and D is the diameter of the receiving field of view of the ocean surface. $\beta_p(\pi)$ and $\beta_w(\pi)$ are the backscattering coefficients of particle and pure seawater, respectively. They can be calculated by the scattering phase function and the scattering coefficient. In this paper $\tilde{\beta}_p(\pi) = 3.154 \times 10^{-3} \text{sr}^{-1}$ [12, 13] and $\tilde{\beta}_w(\pi) = 0.1170 \text{sr}^{-1}$ [13].

In Eq. (5), the K_d is calculated by an empirical relationship between K_d and chlorophyll a concentration $\langle \text{chl} \rangle$,

$$K_d = K_w + \chi \langle \text{chl} \rangle^e \quad (7)$$

where K_w , χ and e are the constants related to the wavelength [14]. The attenuation coefficient c is calculated as a function of $\langle \text{chl} \rangle$

$$\begin{aligned} c_p(\lambda) &= 0.407 \langle \text{chl} \rangle^{0.795} \left(\frac{\lambda}{660} \right)^v \quad (8) \\ v &= \begin{cases} 0.5[\log_{10} \langle \text{chl} \rangle - 0.3], & 0.02 < \text{chl} < 2 \\ 0, & \text{chl} > 2 \end{cases} \end{aligned}$$

2.3. Simulation parameters

The simulator uses the Chl-a concentration profile data set from the Copernicus Marine Environment Monitoring Service (CMEMS) as input to simulate the inherent optical parameters (IOPs) profiles. The CMEMS data combine the BGC-Argo and the MODIS Chl-a concentration data to reconstruct global ocean Chl-a concentration profile data using the neural network method [15]. The performance of various oceanographic lidars deployed on different platforms can be simulated through the simulator by changing the lidar system specifications and environmental parameters. The simulation parameters and algorithm flow of the simulator are shown in Fig. 1.

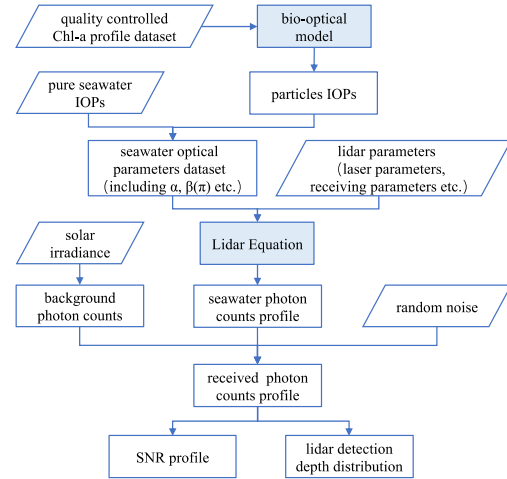


Figure 1. The flowchart of the oceanographic lidar simulator.

3. Verification by airborne lidar

In order to verify the results of the simulator, a real airborne oceanographic lidar data are simulated and compared with the airborne measured data. The bio-optical model parameters are derived from in-situ data.

The airborne lidar system was developed by the Shanghai Institute of Optics and Fine Mechanics, Chinese Academy of Sciences. The flight experiment was conducted in the South China Sea in 2019. During the experiment, the in-situ Chl-a profiles were measured synchronously [16].

The four stations G1, G2, B3 and C2 in the experiment are selected as Li et al., (2020) [16] introduced. The joint experiments of airborne lidar and in-situ measurements were conducted in the South China Sea. The subsurface chlorophyll maximum layers (SCMLs) measured with the in-situ instruments are located at a depth of about 55 m. Above 40 m depth, the seawater is evenly mixed and the Chl-a concentration changes slightly. The input Chl-a concentration profiles of the four stations are shown in Fig. 2.

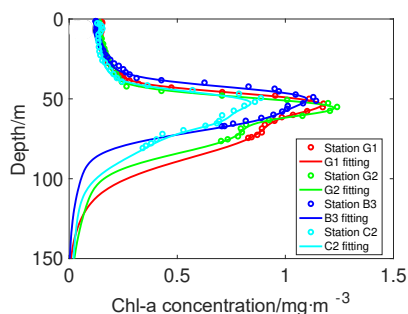


Figure 2. The in-situ Chl-a concentration profiles from stations G1, G2, B3, and C2. The circles are the in-situ measurements, and the solid lines are the gaussian fitting.

The maximum depth of in-situ Chl-a concentration profiles is about 70-80 m. In order to accurately simulate and analyze the detection capability of the lidar, the Chl-a concentration profiles need to be extrapolated. The marine Chl-a concentration profile roughly follows the gaussian distribution, so the profile data with the maximum depth of 150 m are obtained by gaussian fitting [17].

The airborne measurements and simulated results are shown in Fig. 3. The Chl-a concentration increases sharply at the depth of 40-50 m, and a slight bulge is formed based on the simulation profiles. The simulation results and the measured data match well above the depth of the SCMLs, and the agreement gets worse below the depth of SCMLs. The measured and simulated photons show good agreement. The correlation coefficients R^2 reach up to 0.98 in the range of 20 to 70 m. The

difference may due to the uncertainties of the bio-optical model and the temporal difference between the in-situ Chl-a measurements and the lidar flight.

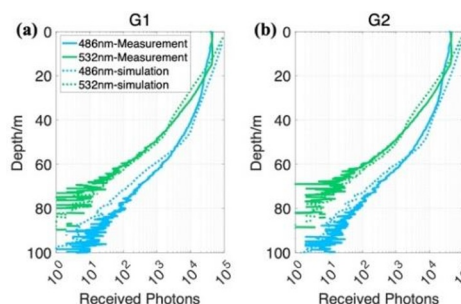


Figure 3. Profiles of measured and simulated photon counts at 486 nm and 532 nm from G1 station and G2 station.

4. Results

According to the lidar equation, the P_{pa} determines most of the performance. The influence of different wavelengths and P_{pa} on the lidar detection capability at night is analyzed. The selected wavelength and P_{pa} combinations are shown in Table 1.

It is shown 443 nm has better penetration capability in the cleanest ocean. The average global lidar penetration capability of 486 nm is better, and there is a solar Fraunhofer dark line near this wavelength, which can effectively reduce the influence of solar background noise on the lidar detection performance. The 532 nm is the most common wavelength and it has better penetration capability than blue light in coastal waters.

Table 1. Specifications and Detection Depths of Spaceborne Lidar

Specifications	Values		
Pulse width/ns	10		
Detection efficiency	0.12		
Orbit height/km	550		
Field of view/mrad	0.3		
P_{pa}/Wm^2	1	10	100
Wavelength/nm	443		
Max depth /m	123.0	158.2	188.9
Mean depth /m	56.9	75.3	96.0
Wavelength/nm	486		
Max depth /m	110.9	150.5	183.4
Mean depth /m	62.6	84.6	109.5
Wavelength/nm	532		
Max depth /m	51.6	73.6	95.6
Mean depth /m	42.5	59.6	76.3

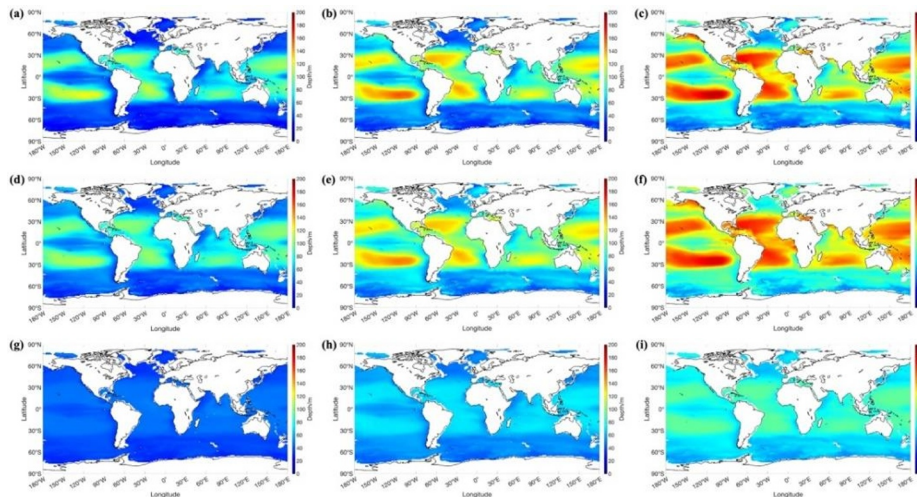


Figure 4. The SPMDD distributions of spaceborne oceanographic lidar. (a), (b), (c) are the SPMDD at 443 nm with P_{pa} of 1, 10, and 100, respectively. Similarly, (d), (e), (f) are the SPMDD at 486 nm, and (g), (h), (i) are at 532 nm.

The simulated SPMDD distributions with typical P_{pa} and wavelengths shown in Fig. 4. The statistical values of the global maximum and average detection depths are shown in Table 1.

5. References

- [1] M.J. Behrenfeld, Y. Hu, C.A. Hostetler, G. Dall’Olmo, S.D. Rodier, J.W. Hair, C.R. Trepte, Space-based lidar measurements of global ocean carbon stocks, *Geophys Res Lett.* **40**, 4355–4360 (2013).
- [2] M.J. Behrenfeld, Y. Hu, R.T. O Malley, E.S. Boss, C.A. Hostetler, D.A. Siegel, J.L. Sarmiento, J. Schulien, J.W. Hair, X. Lu, S. Rodier, A.J. Scarino, Annual boom-bust cycles of polar phytoplankton biomass revealed by space-based lidar, *Nat Geosci.* **10**, 118–122 (2016).
- [3] X. Lu, Y. Hu, Y. Yang, P. Bontempi, A. Omar, R. Baize, Antarctic spring ice-edge blooms observed from space by ICESat-2, *Remote Sens Environ.* **245**, 111827 (2020).
- [4] P. Chen, C. Jamet, Z. Zhang, Y. He, Z. Mao, D. Pan, T. Wang, D. Liu, D. Yuan, Vertical distribution of subsurface phytoplankton layer in South China Sea using airborne lidar, *Remote Sens Environ.* **263**, 112567 (2021).
- [5] J.H. Churnside, Airborne lidar estimates of photosynthesis profiles, in: *International Geoscience and Remote Sensing Symposium (IGARSS)*, Institute of Electrical and Electronics Engineers Inc., 3777–3780 (2021).
- [6] R. Liu, Q. Ling, Q. Zhang, Y. Zhou, C. Le, Y. Chen, Q. Liu, W. Chen, J. Tang, D. Liu, Detection of Chlorophyll a and CDOM Absorption Coefficient with a Dual-Wavelength Oceanic Lidar: Wavelength Optimization Method, *Remote Sens (Basel)*. **12**, 3021 (2020).
- [7] J.H. Churnside, R.D. Marchbanks, Calibration of an airborne oceanographic lidar using ocean backscattering measurements from space, *Opt. Express* **27** A536 (2019).
- [8] J. Churnside, J. Hair, C. Hostetler, A. Scarino, Ocean Backscatter Profiling Using High-Spectral-Resolution Lidar and a Perturbation Retrieval, *Remote Sens (Basel)*. **10** 2003 (2018).
- [9] Z. Liu, P. Voelger, N. Sugimoto, Simulations of the observation of clouds and aerosols with the Experimental Lidar in Space Equipment system, *Appl Opt.* **39**, 3120 (2000).
- [10] K. Chance, R.L. Kurucz, An improved high-resolution solar reference spectrum for earth’s atmosphere measurements in the ultraviolet, visible, and near infrared, *J Quant Spectrosc Radiat Transf.* **111**, 1289–1295 (2010).
- [11] H.R. Gordon, Interpretation of airborne oceanic lidar: effects of multiple scattering, *Appl Opt.* **21**, 2996 (1982).
- [12] T.J. Petzold, Volume scattering functions for selected ocean waters, (UC San Diego: Scripps Institute of Oceanography 1972).
- [13] C.D. Mobley, *The Oceanic Optics Book*, (International Ocean Colour Coordinating Group (IOCCG), Dartmouth, NS, Canada, 2022).
- [14] A. Morel, S. Maritorena, Bio-optical properties of oceanic waters: A reappraisal, *J Geophys Res Oceans.* **106**, 7163–7180 (2001).
- [15] R. Sauzède, H. Claustre, J. Uitz, C. Jamet, G. Dall’Olmo, F. D’Ortenzio, B. Gentili, A. Poteau, C. Schmechtig, A neural network-based method for merging ocean color and Argo data to extend surface bio-optical properties to depth: Retrieval of the particulate backscattering coefficient, *J Geophys Res Oceans.* **121**, 2552–2571 (2016).
- [16] K. Li, Y. He, J. Ma, Z. Jiang, C. Hou, W. Chen, X. Zhu, P. Chen, J. Tang, S. Wu, F. Liu, Y. Luo, Y. Zhang, Y. Chen, A Dual-Wavelength Ocean Lidar for Vertical Profiling of Oceanic Backscatter and Attenuation, *Remote Sens (Basel)*. **12**, 2844 (2020).
- [17] J.J. Cullen, Subsurface Chlorophyll Maximum Layers: Enduring Enigma or Mystery Solved?, *Ann Rev Mar Sci.* **7**, 207–239 (2015).